Spectrochimica Acta Part A: Molecular and Biomolecular Spectroscopy 324 (2025) 124964

Contents lists available at ScienceDirect

Spectrochimica Acta Part A:
Molecular and Biomolecular Spectroscopy

journal homepage: www.journals.elsevier.com/spectrochimica-acta-part-a-molecular-and-biomolecular-spectroscopy

Tailoring refractive index dispersion in ionic liquids: The influence of charge delocalization in cations

Carlos Damián Rodríguez-Fernández [a,*], Alejandro Doval [b], Yago Arosa [b], Héctor González-Núñez [b], Elena López-Lago [b], Raúl de la Fuente [b]

[a] Grupo Mesturas, Departamento de Física e Ciencias da Terra, Universidade da Coruña, Spain
[b] Grupo de Nanomateriais, Fotónica e Materia Branda, Departamento de Física Aplicada, Universidade de Santiago de Compostela, Spain

HIGHLIGHTS

- Molecular polarizability density governs the magnitude of refractive index.
- Aromaticity determines the refractive index dispersion.
- Aliphatic cations and alkyl chains have weak influence in dispersion.
- Aromatic cations produce high refractive index dispersion at short wavelengths.
- Absorption bands related to π orbitals explain the dispersion in aromatic cations.

GRAPHICAL ABSTRACT

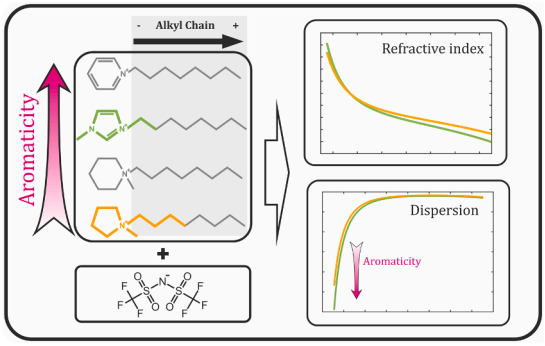

ARTICLE INFO

Keywords:
Ionic liquids
Refractive index
Dispersion
Electronic polarizability
Charge delocalization
Aromaticity
Charge transfer

ABSTRACT

In this work, we study the contributions that different molecular blocks have in the wavelength-dependence of the refractive index in ionic liquids. The ionic liquids chosen for this work are combinations of the bis(trifluoromethylsulfonyl)imide anion with cations based on four different heterocycles with different extents of charge delocalization. The analysis is performed in terms of the experimental electronic polarizability, which is obtained by combining measurements of refractive index curves and densities via the Lorentz-Lorenz equation. Exploiting the additivity of electronic polarizability in ionic liquids, the contribution of the anion and the heterocycles of the cations is separated from that of the alkyl chains. Our results show important differences in these contributions, revealing a key influence of the charge delocalization in the cationic rings on the behavior of the refractive index dispersion. The understanding of how different parts of ionic liquids affect their refractive index dependence on wavelength would allow to gain precise control of this magnitude, enabling the development of customized optical materials for diverse applications in photonics and sensing technologies.

* Corresponding author.
E-mail address: c.damian.rodriguez@udc.es (C.D. Rodríguez-Fernández).

https://doi.org/10.1016/j.saa.2024.124964
Received 5 April 2024; Received in revised form 22 July 2024; Accepted 9 August 2024
Available online 14 August 2024

1. Introduction

Ionic liquids (ILs) have gained significant attention in recent years due to their unique properties and wide-ranging applications in various fields. These versatile fluids, composed entirely of ions, exhibit fascinating characteristics such as low volatility, exceptional solvation ability, and high thermal and electrochemical stabilities [1–4]. Their composition can be easily tuned to obtain liquids with task-specific properties of interest in different research fields. For instance, in the fields of optics and photonics, ILs can be designed to present highly efficient luminescence [5–7], to tailor the response of photonic crystals [8,9], or to maximize their nonlinear optical response [10–13], among others.

Regarding optical properties, refractive index, n, is the cornerstone for the development of optical applications in most photonic devices. In this context, ILs with different refractive indices have been used in variable focal lenses [14–17], liquid-filled waveguides [18,19], immersion liquids [20,21], or for sensing technologies, particularly in the design of optical sensors and biosensors [22,23]. However, ILs not only offer the possibility of designing the refractive index, but also its dependence on wavelength, the refractive index dispersion, $\partial n/\partial \lambda$.

Several works have dealt with the relation of refractive index at a single wavelength (usually n_D, $\lambda = 589$ nm) and the chemical composition of ILs [24–28]. Most of these approaches are based on using the Lorentz-Lorenz equation to transform their density and refractive index into electronic polarizability, since it is linearizable in terms of molecular blocks [29–33]. However, it is possible to expand this single-wavelength formalism to explicitly consider dispersion, a path to understand how the molecular blocks building ILs affect the wavelength dependence of electronic polarizability, and, in the last instance, refractive index curves.

In this paper, we study the way in which different constituent blocks of ILs affect their refractive index and refractive index dispersion, by analyzing their associated electronic polarizability and electronic polarizability dispersion. For this purpose, we measured the density and the refractive index of eleven ILs, all of them based on combinations of the bis(trifluoromethylsulfonyl)imide anion with heterocyclic cations presenting different extents of charge delocalization (aromaticity) in their rings. The measurement of refractive index dispersion was performed on a wide spectral range, from 320 nm to 1700 nm, using Refractive Index Spectroscopy by Broadband Interference (RISBI) [34,35], a white light interferometry-based technique [36,37].

Table 1
ILs studied in this work together with their abbreviation, structure, CAS number and their nominal purity provided by the supplier.

Compound	Abbreviation	Structure	CAS number	Purity
1-Ethyl-3-methylimidazolium bis(trifluoromethylsulfonyl)imide	[C_2mim][NTf_2]		174899-82-2	99 %
1-Butyl-3-methylimidazolium bis(trifluoromethylsulfonyl)imide	[C_4mim][NTf_2]	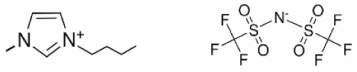	174899-83-3	99 %
1-Hexyl-3-methylimidazolium bis(trifluoromethylsulfonyl)imide	[C_6mim][NTf_2]	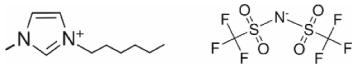	382150-50-7	99 %
1-Methyl-3-octylimidazolium bis(trifluoromethylsulfonyl)imide	[C_8mim][NTf_2]	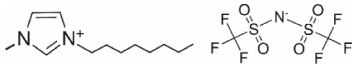	178631-04-4	99 %
1-Butyl-1-methylpyrrolidinium bis(trifluoromethylsulfonyl)imide	[C_4mpyrr][NTf_2]	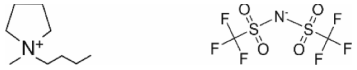	223437-11-4	99 %
1-Hexyl-1-methylpyrrolidinium bis(trifluoromethylsulfonyl)imide	[C_6mpyrr][NTf_2]		380497-19-8	99 %
1-Ethylpyridinium bis(trifluoromethylsulfonyl)imide	[C_2py][NTf_2]	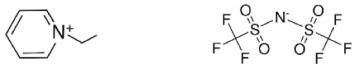	712354-97-7	99 %
1-Butylpyridinium bis(trifluoromethylsulfonyl)imide	[C_4py][NTf_2]	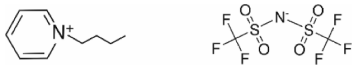	187863-42-9	99 %
1-Hexylpyridinium bis(trifluoromethylsulfonyl)imide	[C_6py][NTf_2]	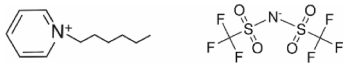	460983-97-5	99 %
1-Methyl-1-propylpiperidinium bis(trifluoromethylsulfonyl)imide	[C_3mpip][NTf_2]		608140-12-1	99 %
1-Butyl-1-methylpiperidinium bis(trifluoromethylsulfonyl)imide	[C_4mpip][NTf_2]	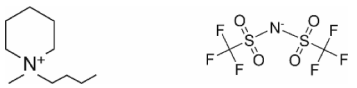	623580-02-9	99 %

2. Materials and methods

2.1. Materials

We have selected eleven ILs sharing the same anion, bis(trifluoromethylsulfonyl)imide, abbreviated as $[NTf_2]^-$, in combination with different cations derived from four types of cationic heterocycles with different aromaticity: 1-akyl-3-methylimidazolium, $[C_k mim]^+$ 1-alkyl-1-methylpyrrolidinium $[C_k mpyrr]^+$, 1-alkylpyridinium, $[C_k py]^+$, and, 1-alkyl-1-methylpiperidinium, $[C_k mpip]^+$. According to the kind of cation, the ILs are divided into four families to facilitate the discussion in the text.

The ILs employed in this work were purchased to Io-Li-Tec, their complete names, abbreviation, structure, CAS Number and purity can be consulted in Table 1. The refractive index and density measurements were done immediately after opening the sealed bottles and without further purification. However, the amount of water in the samples was checked after the measurements using a Mettler-Toledo C10S Coulometric Karl Fischer Titrator. The results have shown a limited absorption of water during manipulation, with water concentration being below 300 ppm in all samples.

2.2. Refractive index

The refractive index curves of the ILs were measured by our RISBI system [35] in the spectral range from 320 nm to 1700 nm. The accuracy of the system is $s(n_{RISBI}) = \pm 2{\cdot}10^{-4}$. All the measurements were performed at 25 °C and 1 atm. In addition, an Atago Multi-Wavelength Abbe Refractometer DR-M2 was also used to characterize the refractive index at five different wavelengths (λ = 486 nm, 546 nm, 589 nm, 633 nm and 680 nm) and used in cooperation with the RISBI system, $s(n_{Abbe}) = \pm 2{\cdot}10^{-4}$.

2.3. Density

To complete the experimental characterization required to estimate electronic polarizability, the densities of the ILs were measured using an Anton Paar DSA-5000 M vibrating tube density and sound velocity meter at the same temperature as that of the measurements of refractive index dispersion, 25 °C. The accuracy of the measurements was $s(\rho) = \pm 1{\cdot}10^{-5}$ g/cm^3.

2.4. Quantum mechanical simulations

Density functional theory (DFT) and time-dependent density functional theory (TD-DFT) calculations were performed using the Gaussian 16 rev. C.01 software [38] at the CAM-B3LYP/6-311++G(d,p) level of theory on isolated ionic pairs (gas phase). The long-range corrected CAM-B3LYP functional was chosen because it has been shown to provide, together with the 6-311++G(d,p) basis set, good results for predicting the electronic polarizability in ILs [33] and a nice performance in TD-DFT calculations [39]. For the TD-DFT calculations of the absorption spectra, a total number of 400 states were simulated, which provided a common minimum wavelength for all the liquids of λ = 115 nm. To analyze the electronic orbitals involved in selected transitions, a Natural Transition Orbital (NTO) analysis was performed [40].

The DFT calculations for estimating the multi-center bond order (MCBO) index of the cationic heterocycles were performed on isolated (gas-phase) cationic species. This parameter was used to quantify the aromaticity throughout their cycles [41–43] and was computed by means of the Multiwfn software [44]. In all cases, the molecular geometry of the systems was previously optimized, and a vibrational analysis was performed to ensure stability.

3. Theory and calculation

The macroscopic polarization density, $P(\lambda)$, describes the reaction of a material of electric susceptibility, $\chi_e(\lambda)$, to the application of an external electric field of wavelength λ, $E_{ext}(\lambda)$. At optical frequencies and low field intensities, the applied electric field induces a linear polarization density, $P(\lambda) = \varepsilon_0\chi_e(\lambda)E_{ext}(\lambda)$, where $\chi_e(\lambda) = \varepsilon_r(\lambda) - 1 = n^2(\lambda) - 1$, being ε_0 the vacuum electric permittivity, $\varepsilon_r(\lambda)$ the relative electric permittivity of the medium and $n(\lambda)$ its refractive index. In consequence, the macroscopic polarization density can be written as $P(\lambda) = \varepsilon_0\left(n^2(\lambda) - 1\right)E_{ext}(\lambda)$, and the refractive index, $n(\lambda)$, is the wavelength-dependent magnitude which relates $P(\lambda)$, with the strength of the applied external field, $E_{ext}(\lambda)$. From the microscopic perspective, the molecules within the material observe an effective or local field, $E_{local}(\lambda)$, which polarizes them according to their electronic polarizability, $\alpha(\lambda)$. The relation between the macroscopic and microscopic responses in the material yields the next expression [45–47]:

$$\left(n^2(\lambda) - 1\right)\varepsilon_0 E_{ext}(\lambda) = N\alpha(\lambda)E_{local}(\lambda), \tag{1}$$

where N is the number density of molecules in the material. If we assume that the action of the local field produces a weak disturbance on the electronic clouds of the molecules around their equilibrium position, they can be described as harmonic oscillators driven by the periodicity of the local electric field. Under these circumstances, the dependence on wavelength of the electronic polarizability of the molecules is described by the Sellmeier model, in which the dispersion is produced by the sum of j resonances, of wavelength λ_j and oscillation strength b_j [45,48]:

$$\alpha(\lambda) = \sum_j b_j \frac{\lambda^2}{\lambda_j^2 - \lambda^2}. \tag{2}$$

Substituting Eq. (2) in Eq. (1), the relation between refractive index and electronic polarizability yields:

$$\left(n^2(\lambda) - 1\right)E_{ext}(\lambda) = \sum_j c_j \frac{\lambda^2}{\lambda_j^2 - \lambda^2}E_{local}(\lambda), \tag{3}$$

where we regrouped all the constants in c_j. Hence, even if we assume a Sellmeier model for the description of the wavelength-dependent response of the material, the specific fashion in which refractive index depends on polarizability is still a function of the relationship between the external and the local electric fields. The most common expression used for describing the refractive index dispersion in dielectric materials is the empirically derived Sellmeier formula, which states:

$$n^2(\lambda) - 1 = \sum_j c_j \frac{\lambda^2}{\lambda_j^2 - \lambda^2}. \tag{4}$$

Hence, in accordance with Eq. (3), in this semi-empirical approach, the local field is identical to the external field, $E_{local}(\lambda) = E_{ext}(\lambda)$. This assumption is reasonable for gases where molecules are very isolated, but not in condensed phases, such as ILs, where ions are expected to be tightly packed. Despite this, Eq. (4) provides, in general, a good performance in condensed media, reason why it is often used for fitting the refractive index curves of solids and liquids [49–51].

One of the expressions most commonly used to describe the local field in liquids is the one derived by Lorentz [46,47]. The Lorentz local field is founded on assuming spherical molecules that perceive the dipoles of the neighboring molecules in addition to the external field. This model is the basis of the Lorenz-Lorenz equation, which is widely used to calculate the polarizability of ILs from refractive index and mass density measurements [29,30,33,52]:

$$\frac{n^2(\lambda) - 1}{n^2(\lambda) + 2} = \frac{N}{3\varepsilon_0}\alpha. \tag{5}$$

Note that in Eq. (5), the number density $N = \rho N_A / M_r$ is directly related with the molecular weight of the IL, M_r; its mass density, ρ; and the Avogadro Number, N_A. Hence, the experimental electronic polarizability at each wavelength, can be readily obtained from this expression using measurements of refractive index curves and mass density.

It has been shown in several articles, that electronic polarizability in ILs is additive in terms of their chemical structure [29,30,52,53], at least when the appropriate building blocks are considered for the linearization [33]. Hence, the electronic polarizability of Eq. (5) can be written as the sum of the polarizabilities of the i molecular blocks composing the IL. Furthermore, according with Eq. (2), the wavelength-dependence of electronic polarizability is the result of the sum of j resonances. Hence, each molecular fragment presents its own contribution to the electronic polarizability curve, Eq. (6):

$$\alpha_{IL}(\lambda) = \sum_i \alpha_i(\lambda) = \sum_i \left(\sum_j f_{ij} \frac{\lambda^2}{\lambda_{ij}^2 - \lambda^2} \right). \tag{6}$$

Eqs. (5) and (6) open a path to tailor the dispersion of refractive index in ILs, going further than other works focused on tailoring the value of refractive index at a single wavelength [29–31,54]. Using Eq. (5), the experimental measurements of density and the refractive index curve can be used to calculate the experimental electronic polarizability curve of a complete IL. Afterwards, exploiting the additivity of electronic polarizability and the structural similitudes among the studied compounds, the electronic polarizability of specific molecular fragments can be isolated and analyzed. Hence, the influence of each part of the IL in both refractive index and refractive index dispersion can be properly identified and exploited to selectively tune the optical behavior of ILs.

4. Results and discussion

4.1. Refractive index and refractive index dispersion

The refractive index curves of the eleven ILs are shown in Fig. 1, and values at selected wavelengths are readily accessible to the reader in Table 2. In case further values were needed, the fitting coefficients of each curve to a Sellmeier formula are provided in Table S1 and the corresponding fitting residuals are shown in Fig. S1, both in the Supporting Information (SI).

The figure shows three main features which are interesting to highlight. First, the refractive indices of the pyridinium-based ILs are larger than those of the rest of families, with independence of the alkyl chain length. Second, in all cases, the refractive index grows with the length of the alkyl chain of the cation, i.e., with k. Please, note that this trend is particular for the liquids upon study, but there are other families of ILs presenting the opposite behavior [29,55]. Third, providing a rigorous list of ILs ordered according to their refractive index values is not a simple task because of the wavelength dependence of this magnitude. Observe that, even if we reduce the comparison to those ILs with the same alkyl chain in the cation, the order depends on the wavelength. For instance, the refractive index of $[C_4mpip][NTf_2]$ is larger in most of the spectrum than that of $[C_4mim][NTf_2]$, but it becomes smaller when approaching to the UV region. As a rough approximation, we could stablish two different lists, one referred to the ultraviolet region ($[C_kpy]^+ > [C_kmim]^+ > [C_kmpip]^+ > [C_kmpyrr]^+$), and the other for the visible and infrared regions ($[C_kpy]^+ > [C_kmpip]^+ > [C_kmim]^+ > [C_kmpyrr]^+$). These lists, despite useful, only reflect the changes in position that dispersion produces, but they do not provide any insight about how dispersion is behaving within each IL. For this reason, a specific analysis on dispersion is needed.

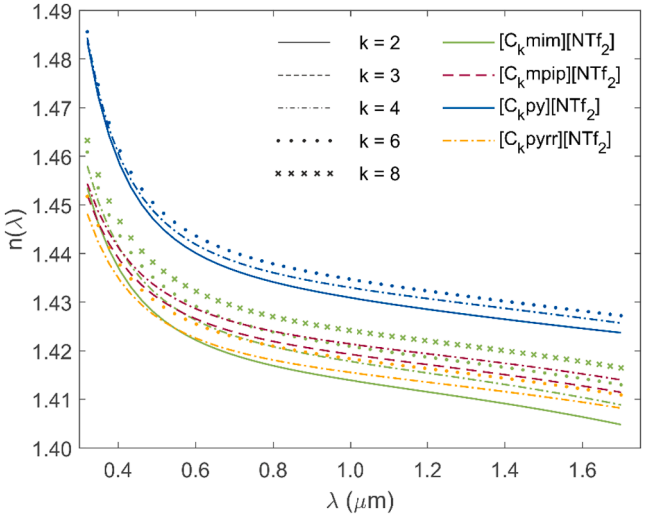

Fig. 1. Refractive index curves of the 11 ILs considered in this work, measured in the spectral range from 320 nm to 1700 nm at 25 °C. The color of line indicates the family of ILs (heterocycle) and the type of the line the alkyl chain length, k.

A rough evaluation of the change of refractive index with wavelength in the visible range is given by the Abbe Number, V_D. It is a magnitude which is often used together with n_D, the refractive index at the sodium D line, to determine the suitability of glasses for a given application in the visible range:

$$V_D = \frac{n_D - 1}{n_F - n_c}, \tag{7}$$

where n_F and n_C are the refractive indices at the spectral lines F and C from hydrogen, $\lambda_F = 486$ nm, and $\lambda_C = 653$ nm. In Fig. 2 these values are shown for all the ILs.

The Abbe number is clearly dependent on the family of ILs upon consideration and presents a slight dependence on the alkyl chain length of the cation. Pyrrolidinium and piperidinium families show the highest Abbe numbers, over 60, which means that they are weakly dispersive, such as glasses based on borosilicates or fluorites. In the opposite direction, imidazolium and, especially pyridinium families, show smaller Abbe numbers and present larger dispersion in the visible range.

Although the Abbe number is commonly used in the design of optical components, certain applications, such as metrology [56] or nonlinear optics [57] require a more precise knowledge of dispersion in a broader spectral range. This more accurate information can be directly retrieved from the refractive index curves by numerically calculating their derivatives with respect to the wavelength, $\partial n/\partial\lambda$, which is the proper definition of chromatic dispersion. This derivative has been obtained from the raw experimental data using a finite differences method with five neighbors to reduce the noise. Fig. 3 shows the dispersion calculated by these means for the members of each family of ILs with an alkyl chain length of $k = 4$.

From this figure, it is clear that chromatic dispersion in these ILs is stronger in the ultraviolet than in the IR, which is the normal trend for most materials. More interestingly, dispersion is similar in all the ILs at the IR, but there are large differences in the UV region. In the IR region, the observed low dispersion of these ILs could be of interest for applications involving zero-dispersion-wavelength. In this regard, in Fig. S2 of the SI we provide the numerical second derivatives of the refractive index, which qualitatively show the zero-dispersion condition. However, more accurate measurements would be needed to characterize this region in a more detailed way. With regard to the UV region, the strongest dispersion is shown by pyridinium and imidazolium ILs, followed by that of piperidinium and pyrrolidinium ILs, whose curves are practically equal and overlapped. These differences in dispersion at short wavelengths are the cause of the differences in the refractive index trends observed in Fig. 1. In the next sections, we address the microscopic origins of this behavior.

Table 2
Refractive index at selected wavelengths and density of the ILs. Sellmeier fits for reproducing the complete refractive index curve are provided in Table S1 and the fitting residuals are shown in Fig. S1 of the SI.

IL	Refractive index at selected wavelengths								*Density*(g/cm^3)
	Ultraviolet		Visible			Infrared			
	320 nm	400 nm	486 nm	589 nm	653 nm	1000 nm	1350 nm	1700 nm	
[C_2mim][NTf_2]	1.4534	1.4372	1.4283	1.4226	1.4203	1.4140	1.4097	1.4050	1.51868
[C_4mim][NTf_2]	1.4580	1.4415	1.4326	1.4267	1.4244	1.4179	1.4136	1.4090	1.43467
[C_6mim][NTf_2]	1.4607	1.4443	1.4354	1.4296	1.4273	1.4209	1.4171	1.4130	1.37245
[C_8mim][NTf_2]	1.4629	1.4473	1.4384	1.4327	1.4304	1.4242	1.4205	1.4164	1.32032
[C_2py][NTf_2]	1.4835	1.4590	1.4476	1.4406	1.4379	1.4308	1.4272	1.4234	1.53506
[C_4py][NTf_2]	1.4845	1.4605	1.4493	1.4424	1.4397	1.4330	1.4293	1.4255	1.44776
[C_6py][NTf_2]	1.4851	1.4620	1.4509	1.4441	1.4415	1.4347	1.4309	1.4269	1.38207
[C_3mpip][NTf_2]	1.4519	1.4391	1.4318	1.4269	1.4249	1.4193	1.4156	1.4114	1.40923
[C_4mpip][NTf_2]	1.4543	1.4413	1.4339	1.4290	1.4270	1.4214	1.4179	1.4141	1.37881
[C_4mpyrr][NTf_2]	1.4481	1.4349	1.4277	1.4230	1.4210	1.4155	1.4121	1.4082	1.39347
[C_6mpyrr][NTf_2]	1.4517	1.4382	1.4308	1.4259	1.4239	1.4184	1.4149	1.4111	1.33612

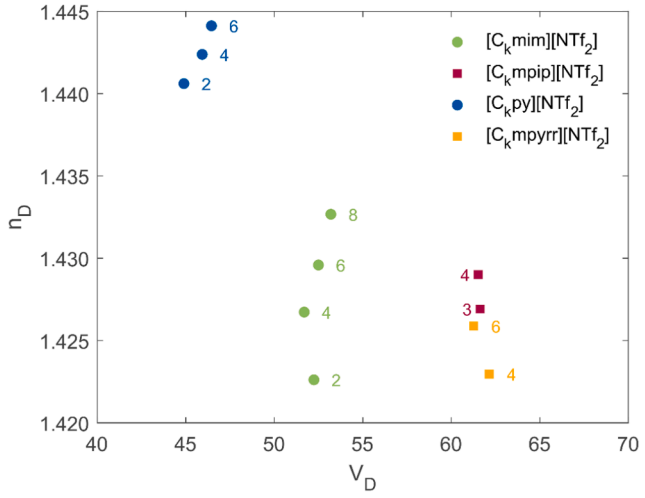

Fig. 2. Abbe diagram of the ILs studied in this work. Numbers indicate *k*, the number of carbons in the alkyl chain attached to the cation of each IL.

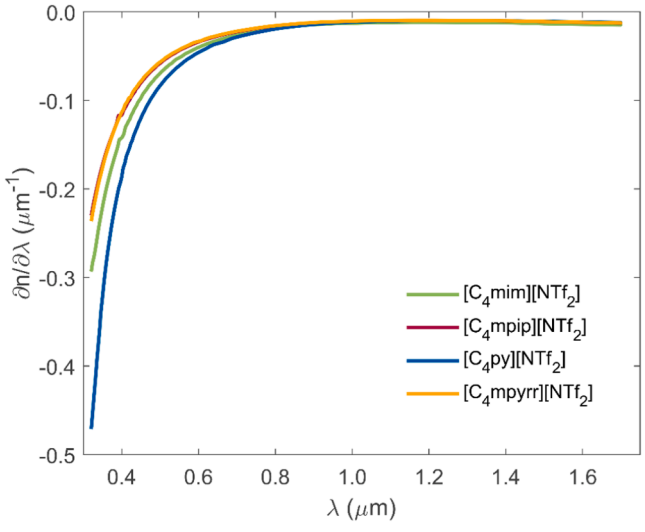

Fig. 3. Numerically calculated chromatic dispersion, $\partial n/\partial\lambda$, obtained from the refractive index curves for those ILs with alkyl chain length $k = 4$.

4.2. Electronic polarizability and molecular polarizability density (MPD)

In general terms, as far as no splitting of conjugated regions is concerned [33], the electronic polarizability of a molecule at a certain wavelength is that arising from the sum of the polarizability of its constituents at that wavelength. The polarizability of each measured IL can be split in two contributions, one coming from its "core", which is the anion and the heterocycle of the cation, and the other coming from the alkyl chain,

$$\alpha_{IL}(\lambda) = \alpha_{core}(\lambda) + \alpha_{alkyl}(\lambda). \quad (8)$$

The contribution from the alkyl chain can be considered as the sum of the polarizability of the k methylene units (–CH_2–) in the chain. Therefore, the alkyl chain contribution to polarizability, denoted as $\alpha_{alkyl}(\lambda)$, can be expressed as $\alpha_{alkyl}(\lambda) = k{\cdot}\alpha_{CH_2}(\lambda)$. This linear relationship between the alkyl electronic polarizability and the chain length allows us to express the overall polarizability of the IL as a linear function of the chain length:

$$\alpha_{IL}(\lambda) = \alpha_{core}(\lambda) + k{\cdot}\alpha_{CH_2}(\lambda). \quad (9)$$

It is important to emphasize that the value of $\alpha_{CH_2}(\lambda)$ could be slightly sensible to chemical environment in the cation alkyl chain [55] as it is the case of the carbon binding energy in X-Ray Photoelectron Spectroscopy (XPS) experiments [58,59]. However, in this work, we take it as a constant, as done in other successful models of polarizability [29,32,53].

Each point in Fig. 4 shows the difference in electronic polarizability at $\lambda = 589$ nm of each IL with respect to the member of its family with alkyl chain length $k = 4$, $\Delta\alpha_{IL}(k) = \alpha_{IL}(k) - \alpha_{IL}(k = 4)$. The same behavior is observed for the rest of wavelengths considered in this work, i.e., the points corresponding to $\Delta\alpha_{IL}(k)$ of the ILs with the same k overlap, and a straight line is always obtained as a function of k. This subtraction serves to remove the core contribution in all the families, which is a common offset to all the electronic polarizability curves, and, hence, it allows to obtain the –CH_2– polarizability from a linear fit using all the liquids at the same time. We have used $k = 4$ in the subtraction because it is the only k common to all the families of liquids in this study, but whatever common k could be used for this purpose. Fig. 4 demonstrates that the methylene groups in the alkyl chain are equivalent in terms of the contribution to the polarizability. It also confirms that $\alpha_{CH_2}(\lambda)$ is a dispersive magnitude but its value at each wavelength is roughly a constant independent of k and the heterocycle to which it is attached to. Hence, Eq. (9) can be safely used to split the contribution of

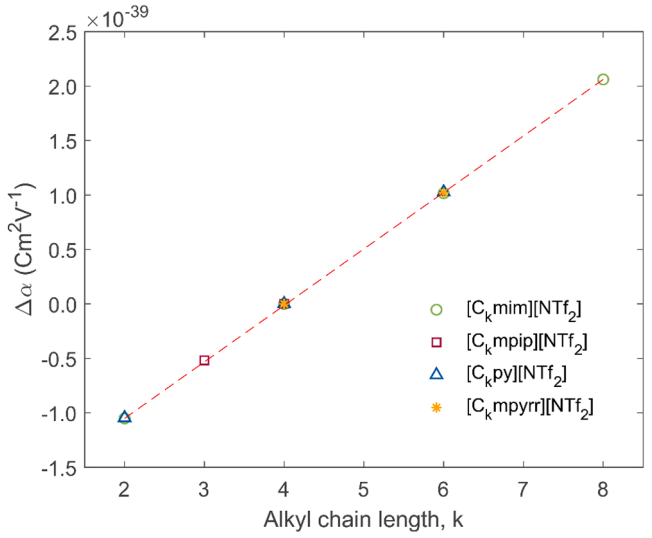

Fig. 4. Increment of the polarizability as function of the alkyl length at $\lambda = 589$ nm for all the ILs. The same behavior is observed at the rest of wavelengths considered in this work.

the core of the IL from that of the alkyl chain, as previously stated.

After fitting the –CH_2– electronic polarizability at each wavelength, a polarizability curve for –CH_2– units is obtained, Fig. 5a). On the other hand, Fig. 5b) shows the curve of the average core polarizability of each family of ILs obtained from subtracting to the polarizability of each IL *k* times the polarizability of the number of –CH_2– units attached to it. Comparing both figures, one could think that the contribution of the –CH_2– unit to the overall polarizability of the IL is very low. However,

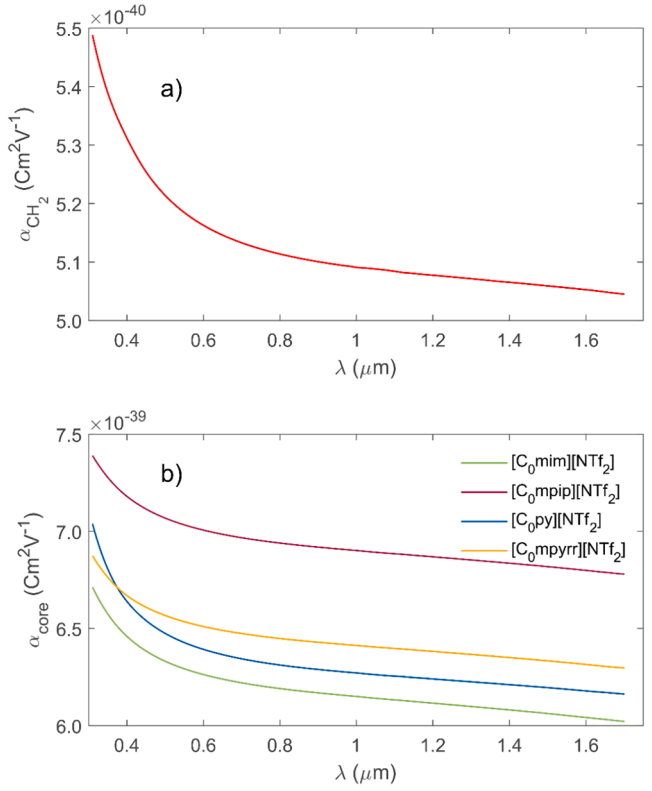

Fig. 5. Experimental curves of a) average electronic polarizability curve of a single methylene group (–CH_2–). b) average electronic polarizability curve of the core of each family of ILs (cationic heterocycle and anion).

since the alkyl chains in ILs can be quite long, the real extent of influence depends on the precise number of –CH_2– units. Readers can find the polarizability values of each core and the –CH_2– unit at selected wavelengths in Table S2 of the SI. Furthermore, the entire polarizability curves were fitted to a Sellmeier formula such as that of Eq. (2), and the fitting coefficients are provided in Table S3 and the corresponding residuals in Figs. S3 and S4.

Another interesting feature to highlight is that the order of cores producing the highest polarizabilities does not coincide with the order observed for the refractive index in those ILs. It was shown in previous articles [29,33] that the ratio between electronic polarizability and molecular volume, i.e., the molecular polarizability density $MPD = \alpha_{IL}/V_{IL}$, is the microscopic magnitude that governs the behavior of the refractive index at the macroscopic scale. Hence, high refractive indices are not produced by high polarizabilities (which is a magnitude that rises with molecular mass), but by high polarizability/molecular volume ratios. The MPD values of the core of ILs upon study, can be calculated following the procedure given in Ref. [33], which is based on the linearization of the molecular volume:

$$V_{IL}(k) = V_{core} + k \cdot V_{CH_2}. \tag{11}$$

After fitting both electronic polarizability and molecular volume for each family of ILs, the MPD values can be extracted by means of the following expression:

$$MPD_{\text{core}} = \frac{\alpha_{core}}{V_{core}}; MPD_{CH2} = \frac{\alpha_{CH2}}{V_{CH2}}. \tag{12}$$

The MPD values of the –CH_2– units and the core of the different families of ILs at three different wavelengths are shown in Table 3.

The MPDs of the cores correlate in almost all the spectral range with the order observed for the refractive index at each wavelength in ILs with the same alkyl chain length (see Table 1), indicating a strong influence of the core MPD in this magnitude. Note that since the –CH_2– units have larger MPD than the cores, increasing the alkyl chain length of the cations will always rise the refractive index of these ILs, in accordance with the behavior observed in Fig. 1. However, the amount of increase depends on how different is the MPD value of the cores and the –CH_2– units. For instance, the unique pair of cores whose MPD and refractive index do not follow the same trend are [C_0mpip][NTf_2] and [C_0mim][NTf_2], at short wavelengths. This discrepancy is produced by alkyl contribution, which changes in a different way the MPD of both cores, as observed for alkyl lengths with k = 4. In the case of $[C_k\text{mpip}]^+$, its structure is almost exclusively composed of –CH_2– units, hence, adding new units will have a different impact on the MPD than the addition of a –CH_2– unit to a conjugated heterocycle like $[C_k\text{mim}]^+$. In fact, according to Refs. [29,55], when the alkyl chain of ILs becomes very long, $k \to \infty$, the MPD of the core becomes negligible, and the MPD of the IL tends to that of an infinite alkane, α_{CH_2}/V_{CH_2}.

An interesting feature to highlight is that, since MPD represents the ratio of polarizability and molecular volume, highest MPD values are associated to higher electronic polarizability densities. It has been

Table 3
Experimental molecular polarizability density (MPD) of the cores of the families of ILs studied and the methylene unit, –CH_2–, at three different wavelengths, and absolute value of the normalized Multi-Center Bond Order (MCBO) Index calculated at the CAM-B3LYP/6-31++G(d,p) level of theory throughout the ring of the cations.

Core	MPD (10^{-12}·$CV^{-1}m^{-1}$)			
	λ = 320 nm	λ = 589 nm	λ = 1700 nm	|MCBO|
[C_0py][NTf_2]	6.98	6.83	6.78	0.65
[C_0mpip][NTf_2]	6.74	6.63	6.58	0.24
[C_0mim][NTf_2]	6.70	6.55	6.50	0.60
[C_0mpyrr][NTf_2]	6.63	6.51	6.47	0.24
–CH_2–	7.27	7.15	7.12	—

exhaustively shown in Ref. [33] that ILs exhibiting charge delocalization present higher polarizability than their aliphatic analogues, while occupying a smaller fraction of volume. In consequence, the presence of charge delocalization tends to increase the MPD of molecules, at least in comparison with their aliphatic homologues. The extent of charge delocalization in a molecule can be estimated through the Multi-Center Bond Order (MCBO) index, a parameter that quantifies conjugation [41–43]. Large values of the MCBO index means large charge delocalization in a cyclic structure while low values indicate aliphatic character. Here, we estimated the MCBO index of the different cationic heterocycles following the procedure described in the Materials and Methods Section. The calculated values are shown in Table 3.

From the data in Table 3, it is clear that the MPD values are largely influenced by the presence of charge delocalization in the heterocycles. The clearest example is pyridinium, which, despite being the species with the smallest molecular weight, presents the highest MPD, much larger than its aliphatic analogue piperidinium. The same observation is also valid for imidazolium and pyrrolidinium cations, being the first one aromatic and the second one aliphatic. Indeed, the MPD of the imidazolium heterocycle is close to that of piperidinium, even if this last one is a larger cation.

4.3. Electronic polarizability dispersion and aromaticity

As in the case of refractive index, the electronic polarizability dispersion, $d\alpha/d\lambda$, was calculated through the numerical derivatives of the experimental α of Fig. 5 with respect to λ. Since we split the polarizability of the ILs in a contribution from the core and another from the $–CH_2–$ unit, we can calculate the dispersion of both magnitudes separately, Fig. 6. In addition, the numeral second derivative of both contributions is also provided in Fig. S5 of the SI.

As expected from what was observed in the refractive index curves, dispersion is very low in the infrared region for all the ILs. On the other hand, major features are observed when the wavelength approaches to the ultraviolet region. There, the $–CH_2–$ unit dispersion is very low in comparison with that of the cores, which are one order of magnitude higher. Among the cores, the piperidinium and the pyrrolidinium cations present low dispersion with almost the same behavior, since their curves are totally superimposed. Conversely, pyridinium and imidazolium cations show larger dispersion, being that of the pyridinium more intense than that of the imidazolium. Indeed, as shown by the dotted lines in Fig. 6, the strength of the dispersion at short wavelengths produced by the core containing pyridinium, is up to twenty times larger than that of the weakly dispersive $–CH_2–$ units.

At this point, it is important to note that the strength of dispersion in the ultraviolet region is tightly related with the extent of charge delocalization established by the MCBO index shown in Table 3. Cations with higher MCBO present higher dispersion in the ultraviolet region in Fig. 6. This finding allows us to associate the strength of the dispersion with the presence of aromaticity in the heterocycles of the cations. Indeed, an extra piece of evidence is that the completely aliphatic heterocycles, piperidinium and pyrrolidinium, do even share the same dispersion curve in the ultraviolet region.

In order to shed more light in this phenomenon, we have simulated by means of TD-DFT the electronic absorption spectra of a member of each IL family, that with $k = 4$, Fig. 7. The simulations were performed according to the specifications described in the section of Materials and Methods.

These calculations show that those ILs that present charge delocalization in their cationic heterocycles exhibit several absorption peaks close to our measurement range. These peaks are absent in the case of the ILs bearing aliphatic heterocycles. From both the Sellmeier description of dispersion given by Eq. (2) or the more general model of the Kramers-Kronig relationships [60], it is clear that absorption peaks produce an increase of electronic polarizability in their surroundings, which explains the differences in dispersion observed for aromatic and aliphatic species at short wavelengths in our measurements. Further insights on this behavior can be provided by analyzing the electronic transitions associated to those absorption peaks. In general, these transitions are complex to describe since they involve several orbitals around the Highest Occupied Molecular Orbital (HOMO) and the Lowest Unoccupied Molecular Orbital (LUMO). For this reason, we employed the NTO approach to simplify the orbital description and to obtain a qualitative picture of the molecular regions participating in the electronic transitions, Fig. S6 of the SI. According with our calculations, the final states of these electronic transitions, (for pyridinium $\lambda = 245$, 236, 226, 197 and 176 nm, and, for imidazolium, λ=198 and 163 nm) are always π^* orbitals located in the aromatic rings, confirming that aromaticity is a key parameter governing dispersion at short wavelengths. The participation of these aromatic molecular regions in similar electronic transitions was already noticed in other calculations [61,62]; however, the tight relation of this aromaticity with the dispersion of the refractive index was not pointed out before, despite it can be a useful tool to design ILs for optical applications.

Furthermore, it is very interesting to mention that most of the origin

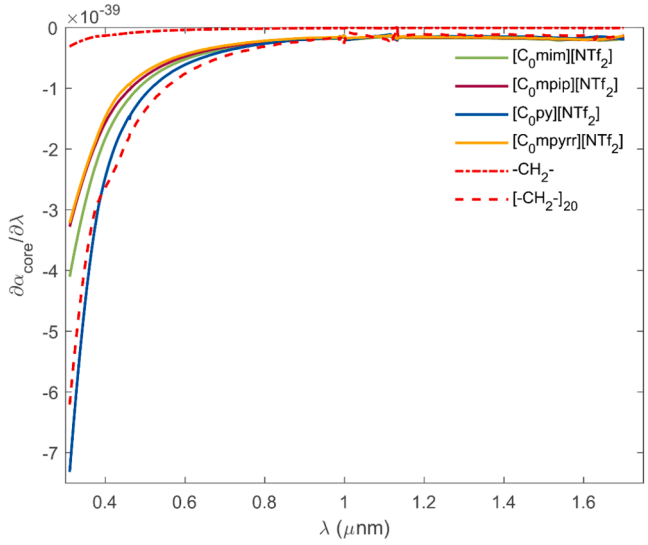

Fig. 6. Electronic polarizability dispersion for the different IL cores and for the $–CH_2–$ group.

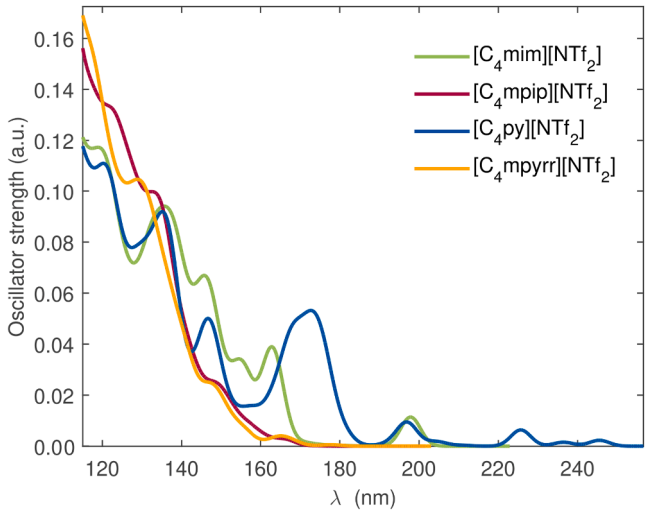

Fig. 7. Absorption spectra simulated by TD-DFT for the members of the different IL families with k = 4.

states of these transitions not only have important contributions from the π orbitals of the aromatic rings, but also from the $[NTf_2]^-$ anion, which is a clear signature of charge transfer between ions. The existence of intermolecular charge transfer was observed in computational works by other authors using a plethora of different levels of theory, such as in Refs. [10,63,64]. However, up to our knowledge, it is the first time that the existence of charge transfer between ions is directly related with the shape of the refractive index dispersion curves in ILs. The impact that these electronic transitions could have on the refractive index dispersion is not clear, but further work is ongoing to analyze the influence of this charge transfer in detail.

5. Conclusions

In this work, we investigated the relationship between the composition of ionic liquids and their refractive index dispersion studying four families of ionic liquids sharing a common anion, bis(trifluoromethylsulfonyl)imide, and differing in the size and aromaticity of the heterocyclic cation (imidazolium, pyridinium, pyrrolidinium and piperidinium). Within each family, the length of the alkyl chain attached to the cation was also considered as an important degree of freedom for the analysis. We expressed the dispersive behavior of refractive index of these liquids in terms of the electronic polarizability dependence on wavelength. Afterwards, we exploited the additivity of electronic polarizability to analyze the contribution that different parts of ionic liquids have on this magnitude and on its dispersion. This methodology is applicable to other families of ionic and non-ionic liquids whose structure is related in such a way that experimental polarizabilities and molecular volumes are linearizable. Note that if this linearization is not possible, the splitting of the total electronic polarizability in the contributions of different molecular blocks is not feasible.

Applying this methodology, we showed that the refractive index of ionic liquids increases with their Molecular Density Polarizability (MPD) while the refractive index dispersion rises with the presence of charge delocalization. Increasing the length of alkyl chains in the studied cations always led to an increase of their refractive index but had a limited impact in dispersion. The reason is that alkyl chains are composed by $–CH_2–$ units, which have larger MPD values than the ionic cores they are attached to, but, on the other hand, they lack of conjugation. However, it is important to note that the specific influence that alkyl chains exert on dispersion depends on the number of $–CH_2–$ units they are made of, since very long chains ($k = 20$) have a contribution like that of the highly dispersive pyridinium cation. The influence of aromaticity in the refractive index dispersion has its origins in electronic transitions involving π and π* orbitals in the cations, which are only present in the imidazolium and pyridinium heterocycles. Our results reveal that the extent of conjugation in ionic liquids plays a fundamental role in the shape of the dispersion, and that it is a key parameter to tune this magnitude. Interestingly, we also found that the presence of aromaticity could favor the transference of charge from the anions to the cations, an effect which foreseeably is highly dependent on the specific ionic pair upon consideration and that we are currently studying.

Our results, yet obtained from a limited set of ionic liquids and focused on the contributions of only a few structural parameters, open a promising path for tailoring the refractive index and refractive index dispersion in these materials. The basic clues described in this work are relevant to design liquids with task-specific refractive response of importance in a variety of optical applications, such as variable lenses, waveguides, filters, or optical sensors. Of course, further work is required to identify the contributions of other common molecular constituents of ionic liquids have on these properties, but we offer here a first step to pave the way for exciting advancements in optical technologies.

Funding sources

This work was funded by Xunta de Galicia and FEDER (GRC 508 ED431C 2020/10). CDRF acknowledges the postdoctoral fellowship ED481B-2024-101 from Xunta de Galicia. AD would like to thank Ministerio de Universidades for the support through the grant FPU21/01302. YA acknowledges the postdoctoral fellowships ED481B-2021-027 and ED481D-2024-001 from Xunta de Galicia. We also thank the Centro de Supercomputación de Galicia (CESGA) facility, Santiago de Compostela, Galicia, Spain, for providing the computational resources employed in this work. Funding for open access charge: Universidade da Coruña/CISUG.

Declaration of competing interest

The authors declare that they have no known competing financial interests or personal relationships that could have appeared to influence the work reported in this paper.

Data availability

Data will be made available on request.

Appendix A. Supplementary data

Supplementary data to this article can be found online at https://doi.org/10.1016/j.saa.2024.124964.

References

[1] M.P. Scott, M. Rahman, C.S. Brazel, Application of ionic liquids as low-volatility plasticizers for PMMA, Eur. Polym. J. 39 (2003) 1947–1953, https://doi.org/10.1016/S0014-3057(03)00129-0.
[2] Y. Cao, T. Mu, Comprehensive investigation on the thermal stability of 66 ionic liquids by thermogravimetric analysis, Ind. Eng. Chem. Res. 53 (2014) 8651–8664, https://doi.org/10.1021/ie5009597.
[3] N. De Vos, C. Maton, C.V. Stevens, Electrochemical stability of ionic liquids: general influences and degradation mechanisms, ChemElectroChem 1 (2014) 1258–1270, https://doi.org/10.1002/celc.201402086.
[4] C. Chiappe, M. Malvaldi, C.S. Pomelli, Ionic liquids: Solvation ability and polarity, Pure Appl. Chem. 81 (2009) 767–776, https://doi.org/10.1351/PAC-CON-08-09-08.
[5] A.-V. Mudring, A. Babai, S. Arenz, R. Giernoth, K. Binnemans, K. Driesen, P. Nockemann, Strong luminescence of rare earth compounds in ionic liquids: Luminescent properties of lanthanide(III) iodides in the ionic liquid 1-dodecyl-3-methylimidazolium bis(trifluoromethanesulfonyl)imide, J. Alloys Compd. 418 (2006) 204–208, https://doi.org/10.1016/j.jallcom.2005.10.069.
[6] S. Tang, A. Babai, A.-V. Mudring, Europium-based ionic liquids as luminescent soft materials, Angew. Chem., Int. Ed. 47 (2008) 7631–7634, https://doi.org/10.1002/anie.200801159.
[7] K. Tanabe, Y. Suzui, M. Hasegawa, T. Kato, Full-color tunable photoluminescent ionic liquid crystals based on tripodal pyridinium, pyrimidinium, and quinolinium salts, J. Am. Chem. Soc. 134 (2012) 5652–5661, https://doi.org/10.1021/ja3001979.
[8] J.Y. Lim, J.B. Ju, D.M. Shin, The chromatic shift of 1-D photonic crystal films influenced by the alkyl group on imidazolium moiety of ionic liquids, Mol. Cryst. Liq. Cryst. 650 (2017) 110–116, https://doi.org/10.1080/15421406.2017.1328227.
[9] H. Zhang, L. Lin, D. Liu, Q. Chen, J. Wu, Optical nose based on porous silicon photonic crystal infiltrated with ionic liquids, Anal. Chim. Acta. 953 (2017) 71–78, https://doi.org/10.1016/j.aca.2016.11.053.
[10] J.E. Castellanos Águila, M. Trejo-Durán, Theoretical study of the second-order nonlinear optical properties of ionic liquids, J. Mol. Liq. 269 (2018) 833–838, https://doi.org/10.1016/j.molliq.2018.08.057.
[11] J.A. Nóvoa-López, E. López Lago, J.A. Seijas, M. Pilar Vázquez-Tato, J. Troncoso, R. de la Fuente, J.R. Salgueiro, H. Michinel, Nonlinear absorption in ionic liquids with transition metallic atoms in the anion, Opt. Mater. (Amst). 52 (2016) 144–149, https://doi.org/10.1016/j.optmat.2015.12.024.
[12] C.D. Rodríguez-Fernández, L.M. Varela, C. Schröder, E.L. Lago, Charge delocalization and hyperpolarizability in ionic liquids, J. Mol. Liq. 349 (2021) 118153, https://doi.org/10.1016/j.molliq.2021.118153.
[13] F. Bardak, C. Bardak, External field intensity and wavelength dependency from IR to deep UV of linear and nonlinear optical properties of 1-butyl-3-methylimidazolium dicyanamide ionic liquid, J. Mol. Liq. 390 (2023) 123014, https://doi.org/10.1016/j.molliq.2023.123014.

[14] X. Hu, S. Zhang, Y. Liu, C. Qu, L. Lu, X. Ma, X. Zhang, Y. Deng, Electrowetting based infrared lens using ionic liquids, Appl. Phys. Lett. 99 (2011) 213505, https://doi.org/10.1063/1.3663633.
[15] X. Hu, S. Zhang, C. Qu, Q. Zhang, L. Lu, X. Ma, X. Zhang, Y. Deng, Ionic liquid based variable focus lenses, Soft Matter 7 (2011) 5941, https://doi.org/10.1039/c1sm05585b.
[16] A. Shahini, J. Xia, Z. Zhou, Y. Zhao, M.-M.-C. Cheng, Versatile miniature tunable liquid lenses using transparent graphene electrodes, Langmuir 32 (2016) 1658–1665, https://doi.org/10.1021/acs.langmuir.5b03407.
[17] S. Calixto, M. Rosete-Aguilar, F. J., O. L., E.M. Martinez Prado, M. Calixto-Solano, Optofluidic compound lenses made with ionic liquids, in: S. Handy (Ed.), Appl. Ion. Liq. Sci. Technol., InTech, 2011. doi:10.5772/24197.
[18] J. Guo, M. Zhou, Y.-G. Liu, K. Di, R. Li, W. Cui, Y. Liu, An all-optical controlled attenuation effect in an all-fiber system based on ionic liquid-filled photonic bandgap fiber, Phys. Scr. 94 (2019) 115508, https://doi.org/10.1088/1402-4896/ab2079.
[19] X. He, Q. Shao, P. Cao, W. Kong, J. Sun, X. Zhang, Y. Deng, Electro-optical phenomena based on ionic liquids in an optofluidic waveguide, Lab Chip 15 (2015) 1311–1319, https://doi.org/10.1039/C4LC01434K.
[20] M. Deetlefs, K.R. Seddon, M. Shara, Neoteric optical media for refractive index determination of gems and minerals, New J. Chem. 30 (2006) 317, https://doi.org/10.1039/b513451j.
[21] X. Wu, M. Muntzeck, T. de los Arcos, G. Grundmeier, R. Wilhelm, T. Wagner, Determination of the refractive indices of ionic liquids by ellipsometry, and their application as immersion liquids, Appl. Opt. 57 (2018) 9215, https://doi.org/10.1364/AO.57.009215.
[22] S.V. Muginova, D.A. Myasnikova, S.G. Kazarian, T.N. Shekhovtsova, Applications of ionic liquids for the development of optical chemical sensors and biosensors, Anal. Sci. 33 (2017) 261–265, https://doi.org/10.2116/analsci.33.261.
[23] R. Marcilla, F. Alcaide, H. Sardon, J.A. Pomposo, C. Pozo-Gonzalo, D. Mecerreyes, Tailor-made polymer electrolytes based upon ionic liquids and their application in all-plastic electrochromic devices, Electrochem. Commun. 8 (2006) 482–488, https://doi.org/10.1016/j.elecom.2006.01.013.
[24] S. Seki, S. Tsuzuki, K. Hayamizu, Y. Umebayashi, N. Serizawa, K. Takei, H. Miyashiro, Comprehensive refractive index property for room-temperature ionic liquids, J. Chem. Eng. Data 57 (2012) 2211–2216, https://doi.org/10.1021/je201289w.
[25] K. Moutzouris, M. Papamichael, S.C. Betsis, I. Stavrakas, G. Hloupis, D. Triantis, Refractive, dispersive and thermo-optic properties of twelve organic solvents in the visible and near-infrared, Appl. Phys. B 116 (2014) 617–622, https://doi.org/10.1007/s00340-013-5744-3.
[26] M. Tariq, P.A.S. Forte, M.F.C. Gomes, J.N.C. Lopes, L.P.N. Rebelo, Densities and refractive indices of imidazolium- and phosphonium-based ionic liquids: Effect of temperature, alkyl chain length, and anion, J. Chem. Thermodyn. 41 (2009) 790–798, https://doi.org/10.1016/j.jct.2009.01.012.
[27] M. Dzida, M. Musiał, E. Zorębski, M. Zorębski, J. Jacquemin, P. Goodrich, Z. Wojnarowska, M. Paluch, Comparative study of effect of alkyl chain length on thermophysical characteristics of five N-alkylpyridinium bis (trifluoromethylsulfonyl)imides with selected imidazolium-based ionic liquids, J. Mol. Liq. 278 (2019) 401–412, https://doi.org/10.1016/j.molliq.2019.01.022.
[28] G. Vakili-Nezhaad, M. Vatani, M. Asghari, I. Ashour, Effect of temperature on the physical properties of 1-butyl-3-methylimidazolium based ionic liquids with thiocyanate and tetrafluoroborate anions, and 1-hexyl-3-methylimidazolium with tetrafluoroborate and hexafluorophosphate anions, J. Chem. Thermodyn. 54 (2012) 148–154, https://doi.org/10.1016/j.jct.2012.03.024.
[29] K. Bica, M. Deetlefs, C. Schröder, K.R. Seddon, Polarisabilities of alkylimidazolium ionic liquids, Phys. Chem. Chem. Phys. 15 (2013) 2703, https://doi.org/10.1039/c3cp43867h.
[30] C.E.S. Bernardes, K. Shimizu, J.N.C. Lopes, P. Marquetand, E. Heid, O. Steinhauser, C. Schröder, Additive polarizabilities in ionic liquids, Phys. Chem. Chem. Phys. 18 (2016) 1665–1670, https://doi.org/10.1039/c5cp06595j.
[31] P. Díaz-Rodríguez, J.C. Cancilla, N.V. Plechkova, G. Matute, K.R. Seddon, J. S. Torrecilla, Estimation of the refractive indices of imidazolium-based ionic liquids using their polarisability values, Phys. Chem. Chem. Phys. 16 (2014) 128–134, https://doi.org/10.1039/C3CP53685H.
[32] S. Koutsoumpos, M. Chronaki, C. Tsonos, T. Karakasidis, L. Guazzelli, A. Mezzetta, K. Moutzouris, On the application of the Wildman-Crippen model to ionic liquids, Results Mater. 16 (2022) 100350, https://doi.org/10.1016/j.rinma.2022.100350.
[33] C.D. Rodríguez-Fernández, E. López Lago, C. Schröder, L.M. Varela, Non-additive electronic polarizabilities of ionic liquids: Charge delocalization effects, J. Mol. Liq. 346 (2022) 117099, https://doi.org/10.1016/j.molliq.2021.117099.
[34] Y. Arosa, PhD Thesis: Spectroscopic refractometry by broadband interference within the ultraviolet, visible and near infrared ranges, Universidade de Santiago de Compostela, 2019 https://investigacion.usc.gal/documentos/5dc161432999520980ece560?lang=es (accessed September 13, 2023).
[35] Y. Arosa, E.L. Lago, L.M. Varela, R. de la Fuente, Spectrally resolved white light interferometry to measure material dispersion over a wide spectral band in a single acquisition, Opt. Express. 24 (2016) 17303, https://doi.org/10.1364/OE.24.017303.
[36] M. Galli, F. Marabelli, G. Guizzetti, Direct measurement of refractive-index dispersion of transparent media by white-light interferometry, Appl. Opt. 42 (2003) 3910, https://doi.org/10.1364/AO.42.003910.
[37] Y.-S. Ghim, S.-W. Kim, Thin-film thickness profile and its refractive index measurements by dispersive white-light interferometry, Opt. Express. 14 (2006) 11885, https://doi.org/10.1364/OE.14.011885.
[38] M.J. Frisch, G.W. Trucks, H.B. Schlegel, G.E. Scuseria, M. a. Robb, J.R. Cheeseman, G. Scalmani, V. Barone, G. a. Petersson, H. Nakatsuji, X. Li, M. Caricato, a. V. Marenich, J. Bloino, B.G. Janesko, R. Gomperts, B. Mennucci, H.P. Hratchian, J. V. Ortiz, a. F. Izmaylov, J.L. Sonnenberg, Williams, F. Ding, F. Lipparini, F. Egidi, J. Goings, B. Peng, A. Petrone, T. Henderson, D. Ranasinghe, V.G. Zakrzewski, J. Gao, N. Rega, G. Zheng, W. Liang, M. Hada, M. Ehara, K. Toyota, R. Fukuda, J. Hasegawa, M. Ishida, T. Nakajima, Y. Honda, O. Kitao, H. Nakai, T. Vreven, K. Throssell, J. a. Montgomery Jr., J.E. Peralta, F. Ogliaro, M.J. Bearpark, J.J. Heyd, E.N. Brothers, K.N. Kudin, V.N. Staroverov, T. a. Keith, R. Kobayashi, J. Normand, K. Raghavachari, a. P. Rendell, J.C. Burant, S.S. Iyengar, J. Tomasi, M. Cossi, J.M. Millam, M. Klene, C. Adamo, R. Cammi, J.W. Ochterski, R.L. Martin, K. Morokuma, O. Farkas, J.B. Foresman, D.J. Fox, Gaussian 16, Revision C.01, Gaussian Inc. Wallingford CT, 2016.
[39] C. Adamo, D. Jacquemin, The calculations of excited-state properties with Time-Dependent Density Functional Theory, Chem. Soc. Rev. 42 (2013) 845–856, https://doi.org/10.1039/C2CS35394F.
[40] R.L. Martin, Natural transition orbitals, J. Chem. Phys. 118 (2003) 4775–4777, https://doi.org/10.1063/1.1558471.
[41] M. Giambiagi, M.S. de Giambiagi, K.C. Mundim, Definition of a multicenter bond index, Struct. Chem. 1 (1990) 423–427, https://doi.org/10.1007/BF00671228.
[42] R. Ponec, P. Bultinck, A.G. Saliner, Multicenter bond indices as a new means for the quantitative characterization of homoaromaticity, J. Phys. Chem. A. 109 (2005) 6606–6609, https://doi.org/10.1021/jp052179b.
[43] P. Bultinck, R. Ponec, S. Van Damme, Multicenter bond indices as a new measure of aromaticity in polycyclic aromatic hydrocarbons, J. Phys. Org. Chem. 18 (2005) 706–718, https://doi.org/10.1002/poc.922.
[44] T. Lu, F. Chen, Multiwfn: A multifunctional wavefunction analyzer, J. Comput. Chem. 33 (2012) 580–592, https://doi.org/10.1002/jcc.22885.
[45] E. Hecht, Optics, Pearson, 2012.
[46] H. Kragh, The Lorenz-Lorentz formula: origin and early history, Substantia 2 (2018) 7–18, https://doi.org/10.13128/Substantia-56.
[47] B.J. Hoenders, The painful derivation of the refractive index from microscopical considerations, in: 2008: pp. 297–305. doi:10.1007/978-0-387-71809-5_30.
[48] W. Sellmeier, Ueber die durch die Aetherschwingungen erregten Mitschwingungen der Körpertheilchen und deren Rückwirkung auf die ersteren, besonders zur Erklärung der Dispersion und ihrer Anomalien, Ann. Der Phys. Und Chemie. 223 (1872) 386–403, https://doi.org/10.1002/andp.18722231105.
[49] J.W. Fleming, Dispersion in GeO_2–SiO_2 glasses, Appl. Opt. 23 (1984) 4486, https://doi.org/10.1364/AO.23.004486.
[50] G. Ghosh, M. Endo, T. Iwasaki, Temperature-dependent Sellmeier coefficients and chromatic dispersions for some optical fiber glasses, J. Light. Technol. 12 (1994) 1338–1342, https://doi.org/10.1109/50.317500.
[51] C.D. Rodríguez Fernández, Y. Arosa, B. Algnamat, E. López Lago, R. de la Fuente, An experimental and computational study on the material dispersion of 1-alkyl-3-methylimidazolium tetrafluoroborate ionic liquids, Phys. Chem. Chem. Phys. 22 (2020) 14061–14076, https://doi.org/10.1039/D0CP01572E.
[52] E. Heid, A. Szabadi, C. Schröder, Quantum mechanical determination of atomic polarizabilities of ionic liquids, Phys. Chem. Chem. Phys. 20 (2018) 10992–10996, https://doi.org/10.1039/c8cp01677a.
[53] S.A. Wildman, G.M. Crippen, Prediction of Physicochemical Parameters by Atomic Contributions, J. Chem. Inf. Comput. Sci. 39 (1999) 868–873, https://doi.org/10.1021/ci990307l.
[54] M. Sattari, A. Kamari, A.H. Mohammadi, D. Ramjugernath, Prediction of refractive indices of ionic liquids – A quantitative structure-property relationship based model, J. Taiwan Inst. Chem. Eng. 52 (2015) 165–180, https://doi.org/10.1016/j.jtice.2015.02.003.
[55] B.S. Algnamat, Y. Arosa, E. López Lago, R. de la Fuente, An inspection of the dispersive properties of imidazolium-based ionic liquids in the Vis-NIR, Opt. Mater. (amst). 102 (2020) 109764, https://doi.org/10.1016/j.optmat.2020.109764.
[56] T. Yoshizawa (Ed.), Handbook of Optical Metrology, CRC Press, 2009, https://doi.org/10.1201/9781420019513.
[57] B.E.A. Saleh, M.C. Teich, Fundamentals of Photonics, Wiley (1991), https://doi.org/10.1002/0471213748.
[58] S. Men, D.S. Mitchell, K.R.J. Lovelock, P. Licence, X-ray photoelectron spectroscopy of pyridinium-based ionic liquids: comparison to imidazolium- and pyrrolidinium-based analogues, ChemPhysChem 16 (2015) 2211–2218, https://doi.org/10.1002/cphc.201500227.
[59] S. Men, P. Licence, C.L. Do-Thanh, H. Luo, S. Dai, X-ray photoelectron spectroscopy of piperidinium ionic liquids: a comparison to the charge delocalised pyridinium analogues, Phys. Chem. Chem. Phys. 22 (2020) 11976–11983, https://doi.org/10.1039/d0cp01454k.
[60] L. Valerio., P. Kai-Erik, J.J. Saarinen, V. Erik M., Kramers-Kronig relations in optical materials research, Springer-Verlag, Berlin/Heidelberg, 2005. doi:10.1007/b138913.

[61] I. Tanabe, Y. Kurawaki, Y. Morisawa, Y. Ozaki, Electronic absorption spectra of imidazolium-based ionic liquids studied by far-ultraviolet spectroscopy and quantum chemical calculations, Phys. Chem. Chem. Phys. 18 (2016) 22526–22530, https://doi.org/10.1039/C6CP02930B.

[62] J.E. Castellanos-Águila, M.A. Olea-Amezcua, H. Hernández-Cocoletzi, M. Trejo-Durán, Tuning the nonlinear optical properties of the $[alkyl\text{-}Py]^{+}[NO_3]^{-}$ and $[alkyl\text{-}MIM]^{+}[NO_3]^{-}$ ionic liquids, J. Mol. Liq. 285 (2019) 803–810, https://doi.org/10.1016/j.molliq.2019.04.075.

[63] F. Bardak, C. Bardak, C. Karaca, E. Kose, S. Bilgili, A. Atac, Anionic dependency of electronic and nonlinear optical properties of ionic liquids, J. Mol. Liq. (2021) 117030, https://doi.org/10.1016/j.molliq.2021.117030.

[64] Z. Fakhri, A. Soltanabadi, S. Kiani, A. Maleki, A theoretical study of the comparison of gas-phase electronic properties and structure of pyridinium-based ionic liquids with different anions (chloride, bromide and iodide), Theor. Chem. Acc. 143 (2024) 42, https://doi.org/10.1007/s00214-024-03118-9.